JACS
JOURNAL OF THE AMERICAN CHEMICAL SOCIETY

Communication

pubs.acs.org/JACS

Photoelectric Covalent Organic Frameworks: Converting Open Lattices into Ordered Donor–Acceptor Heterojunctions

Long Chen,[†,‡] Ko Furukawa,[§] Jia Gao,[‡] Atsushi Nagai,[‡] Toshikazu Nakamura,[‡] Yuping Dong,[†] and Donglin Jiang*[,‡]

[†]College of Materials Science and Engineering, Beijing Institute of Technology, 5 South Zhongguancun Street, Haidian District, Beijing 100081, China

[‡]Department of Materials Molecular Science, Institute for Molecular Science, National Institutes of Natural Sciences, 5-1 Higashiyama, Myodaiji, Okazaki 444-8787, Japan

[§]Institute for Research Promotion Center for Instrumental Analysis, Niigata University, 8050 Ikarashi, 2 Nocho, Niigata-city, Niigata 950-2181, Japan

Supporting Information

ABSTRACT: Ordered one-dimensional open channels represent the typical porous structure of two-dimensional covalent organic frameworks (COFs). Here we report a general synthetic strategy for converting these open lattice structures into ordered donor–acceptor heterojunctions. A three-component topological design scheme was explored to prepare electron-donating intermediate COFs, which upon click reaction were transformed to photoelectric COFs with segregated donor–acceptor alignments, whereas electron-accepting buckyballs were spatially confined within the nanochannels via covalent anchoring on the channel walls. The donor–acceptor heterojunctions trigger photoinduced electron transfer and allow charge separation with radical species delocalized in the π-arrays, whereas the charge separation efficiency was dependent on the buckyball content. This new donor–acceptor strategy explores both skeletons and pores of COFs for charge separation and photoenergy conversion.

Covalent organic frameworks (COFs) have emerged as a new class of crystalline porous architectures that allow atomically precise integration of desirable π-building blocks into periodic columnar arrays in bulky solids and thin films.[1−7] Two-dimensional (2D) COFs induce a large electronic coupling between the π-orbitals of the eclipsed stacking sheets, which facilitate charge carrier transport through the preorganized π-pathways.[1,3−5] The 2D COFs offer a new platform for the molecular design of semiconducting and photoconductive materials. In particular, exploration of synthetic strategies for the construction of COFs with electron donor and acceptor components is crucial for photoinduced electron transfer and photoenergy conversion.[5b]

Two strategies have been established for the synthesis of donor–acceptor COFs.[4,5] By using electron donor and acceptor as monomers, we have developed a covalent methodology for the synthesis of donor–acceptor COFs, whereas the skeletons are built from alternately linked donor and acceptor π-arrays and leave open channels unused.[4] As an alternative way, we and other groups have explored a supramolecular approach by spatially confining electron acceptors within the open channels of electron-donating frameworks.[5] Clearly, the former approach requires a planar conformation of the monomer units and is not applicable to the zero-dimensional molecules, such as buckyballs, a class of widely utilized electron acceptors. The second approach based on physical filling can load buckyballs; however, it encounters a problem on the fullerene elution from the channels. By using a three-component topological design diagram in conjunction with click chemistry, we developed a method for converting the open lattice of COFs into photoelectric structures that are covalently linked with ordered donor–acceptor arrays.

We employed a three-component condensation system of (2,3,9,10,16,17,23,24-octahydroxyphthalocyaninato)zinc (ZnPc[OH]$_8$) as vertices and 1,4-phenylenediboronic acid (BDBA) and 2,5-bis(azidomethyl)-1,4-phenylenediboronic acid (N_3-BDBA) at different molar ratios as edges under solvothermal conditions for the synthesis of a series of electron-donating intermediate ZnPc-COFs with different contents of the azide units on the channel walls (Chart 1A, X %N_3-ZnPc-COFs, X = 0, 10, 25, and 50, N_3 = azide unit).[6] The condensation reactions exhibited similar isolated yields to each other, indicating that the reactivity of BDBA and N_3-BDBA is similar under solvothermal conditions (Supporting Information, SI). This feature also suggests that the azide units are homogeneously distributed on the channel walls of the COFs. The edge units of X%N_3-ZnPc-COFs consist of azido methylphenyl group and phenyl unit at a molar ratio of 0/100, 10/90, 25/75, and 50/50, respectively. The azide units undergo click reaction with alkynes, such as 1,2-(4′-propiolyloxycyclohexno) fullerene, which covalently links the fullerene moieties onto the channel walls via 1,2,3-triazole units (Chart 1A, [C_{60}]$_y$-ZnPc-COFs; y = [C_{60}]/[ZnPc] = 0.3, 0.4, and 0.5). Phthalocyanines and fullerenes are widely studied donor–acceptor systems; various supermolecules have been developed for achieving ordered structures.[8] In this study, we explored channel confinement and lattice ordering of COFs as an alternative way toward organizing donor and acceptor into

Received: March 17, 2014
Published: June 25, 2014

   dx.doi.org/10.1021/ja502692w | J. Am. Chem. Soc. 2014, 136, 9806−9809

Chart 1. (A) Schematic Representation of Converting Open Lattice Structures into Segregated Donor–Acceptor Arrays and (B) Top and Side Views of Donor–Acceptor COF with C_{60} (purple) Integrated on the Channel Walls[a]

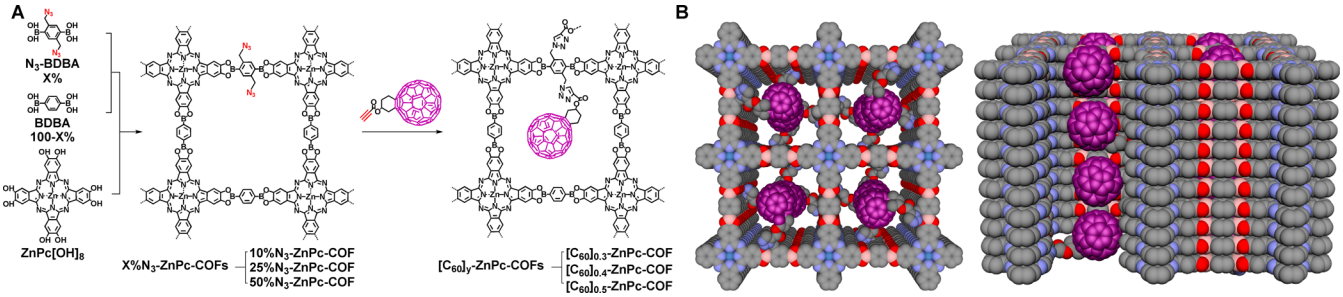

[a]In the side view, the one column of edge units was removed for illustration of C_{60} alignment.

ordered system. The COFs were characterized by various spectroscopy (Figures S1, S2), elemental analysis (SI), electron microscopy (Figures S3, S4), and X-ray diffraction (XRD) measurements.

Infrared (IR) spectroscopy provided direct evidence for the presence of azide units in X%N_3-ZnPc-COFs and fullerene units in $[C_{60}]_y$-ZnPc-COFs, as evidenced by vibration bands at 2104 and 1713 cm^{-1} for the azide and C═O units, respectively (Figure S1, Table S1). After click reaction, the resulting COF from 10%N_3-ZnPc-COF did not exhibit the signal of the azide unit. This observation indicates that the azide units are transformed almost completely. In sharp contrast, when the azide content was 25% and 50%, the resulting COFs still exhibited the vibration bands of the azide units. As a result of steric hindrance of the C_{60} units, only portion of azide units in 25%N_3-ZnPc-COF and 50%N_3-ZnPc-COF reacts with 1,2-(4′-propiolyloxycyclohexno) fullerene. To evaluate the C_{60} content in $[C_{60}]_y$-ZnPc-COFs, we utilized a standard method based on electronic absorption spectroscopy (Figure S8). As a result, the C_{60} content (y) was estimated to be 0.3, 0.4, and 0.5 for the COFs prepared from 10%N_3-ZnPc-COF, 25%N_3-ZnPc-COF, and 50%N_3-ZnPc-COF, respectively. Considering the pore size (2.2 nm) and interlayer distance (3.36 Å) of ZnPc-COF (see below), the size of fullerene (7.0 Å), and the linker length, $[C_{60}]_y$-ZnPc-COFs likely accommodate fullerene molecules in a peapod-like mode within the nanochannels (Chart 1B).

To characterize the crystalline structure, XRD measurements were conducted. X%N_3-ZnPc-COFs exhibited almost same XRD patterns in both peak position and relative intensity (Figures 1 and S5), irrespective of the azide content; they gave a strong peak at 3.8° together with relatively weak signals at 7.7, 11.7, and 26.7°, which were assigned to the 100, 200, 300, and 001 facets, respectively. Therefore, X%N_3-ZnPc-COFs assume the same 0.8-Å slipped AA stacking crystalline structure as that of ZnPc-COF.[3f] The unit cell is $P1$ space group with the parameter of $a = b = 23.12$ Å, $c = 6.72$ Å, and $\alpha = \beta = \gamma = 90°$.

$[C_{60}]_y$-ZnPc-COFs exhibited the XRD peaks with same positions as X%N_3-ZnPc-COFs; signals for the 100, 200, 300, and 001 facets are retained, and no new XRD peaks were observed (Figures 1 and S5). In particular, the interlayer distance of the COFs did not change upon click reaction (Figure 1, inset). It should also be noted that a decrease in the XRD intensity was observed. Similar observations were reported for other COFs that were caused by amorphous alkyl chains on the walls or guest molecules loaded within the pores; the decreased intensity dose not reflect the deteriorated crystallinity of the COF skeleton itself.[6,7]

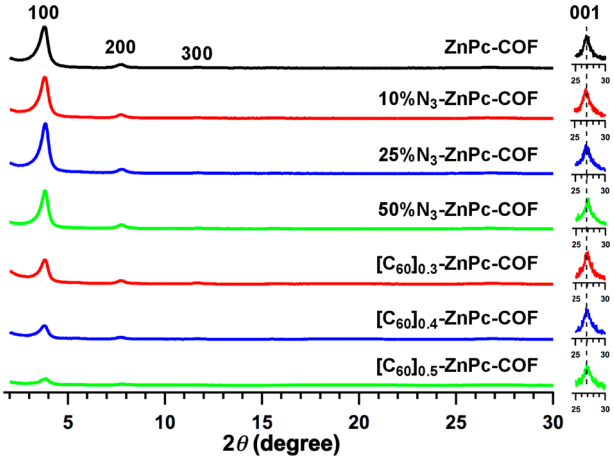

Figure 1. PXRD patterns for ZnPc-COF, X%N_3-ZnPc-COFs, and $[C_{60}]_y$-ZnPc-COFs. Insets are the 001 peaks.

To investigate how the porosity changes, nitrogen sorption isotherm measurements were conducted at 77 K. X%N_3-ZnPc-COFs exhibited type-I sorption curves (Figure 2A), which are characteristics of mesoporous materials. Interestingly, their

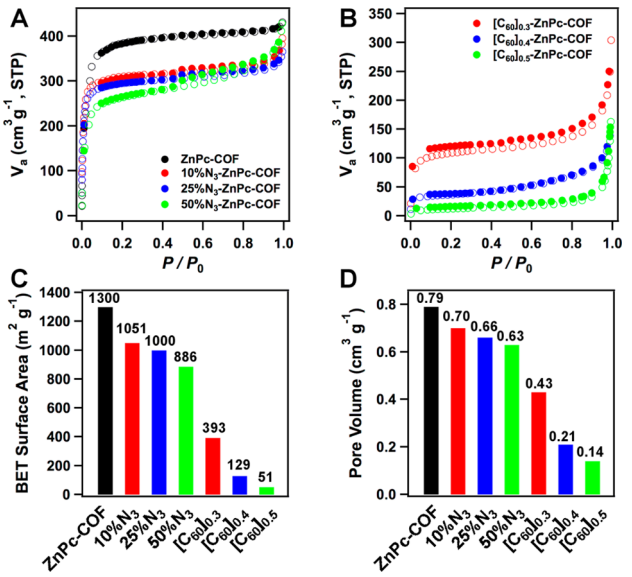

Figure 2. N_2 sorption isotherms of (A) X%N_3-ZnPc-COFs and (B) $[C_{60}]_y$-ZnPc-COFs measured at 77 K; (C) BET surface area; and (D) the pore volume of the COFs.

dx.doi.org/10.1021/ja502692w | J. Am. Chem. Soc. 2014, 136, 9806–9809

surface area and pore volume exhibited a decrease tendency as the azide content was increased. Brunauer–Emmett–Teller (BET) surface area was 1300, 1051, 1000, and 886 $m^2\ g^{-1}$ for ZnPc-COF, 10%N_3-ZnPc-COF, 25%N_3-ZnPc-COF, and 50% N_3-ZnPc-COF, respectively (Figure 2C). Pore size distribution profiles (Figure S6) revealed that each X%N_3-ZnPc-COF consists of only one kind of mesopore. The pore volume decreased from 0.79 to 0.70, 0.66, and 0.63 $cm^3\ g^{-1}$ as the azide content was increased from 0% to 10%, 25%, and 50% (Figure 2D, Table S2).

Upon covalent integration of fullerene onto the channel walls, $[C_{60}]_y$-ZnPc-COFs exhibited a much more drastic drop in BET surface area, and pore volume as the fullerene content was increased (Figure 2B). The $[C_{60}]_{0.3}$-ZnPc-COF sample has a BET surface area and pore volume of 393 $m^2\ g^{-1}$ and 0.43 $cm^3\ g^{-1}$, respectively, which decreased sharply to 129 $m^2\ g^{-1}$ and 0.21 $cm^3\ g^{-1}$ for $[C_{60}]_{0.4}$-ZnPc-COF and 51 $m^2\ g^{-1}$ and 0.14 $cm^3\ g^{-1}$ for $[C_{60}]_{0.5}$-ZnPc-COF (Figure 2C,D). Integration of fullerene onto the channel walls drastically decreases the free space for the nitrogen sorption.

Fullerene units have an absorption band centered at 451 nm, which are complementary to the absorbance of ZnPc-COF centered in the near-IR region (Figure S7). This feature endows $[C_{60}]_y$-ZnPc-COFs with strong light absorbance covering from visible region to IR zone as long as 1200 nm. A broad and strong light absorbance is important because the sunlight provides a low-density irradiance of about 1 kW m^{-2} at sea level and the major (>97%) of the solar energy is in the form of visible and IR irradiations. Compared with X%N_3-ZnPc-COFs, the enhancement of the absorbance at 451 nm was 17%, 41%, and 56% for $[C_{60}]_{0.3}$-ZnPc-COFs, $[C_{60}]_{0.4}$-ZnPc-COF, and $[C_{60}]_{0.5}$-ZnPc-COF, respectively. The higher the fullerene content is, the stronger the absorbance of the visible photons shows.

Because these COFs are not luminescent, we investigated the photoinduced electron transfer and revealed the charge dynamics of the donor–acceptor COFs in the solid state by using time-resolved electron spin resonance (TR-ESR) spectroscopy (Figure 3). Upon the laser flash at 680 nm, the electron-donating ZnPc-COF at 20 K without fullerene acceptors on the walls exhibited only broad TR-ESR signal ranged from 0.315 to 0.380 T (Figure 3A). In order to interpret the observed spectrum, we performed the spectral simulation by using the spin Hamiltonian expressed by the summation of Zeemann and zero-field splitting terms. The simulated spectrum (Figure 3B, green curve) is in good agreement with the experimentally observed one (red curve), which suggests that the observed ESR signal originates from the excited triplet state. Therefore, in the absence of fullerene acceptors, light irradiation generates the excited triplet states without the generation of charge-separated states.

Integrating of electron-accepting fullerene molecules onto the channel walls drastically changes the TR-ESR patterns; the broad TR-ESR signal of the ZnPc-COF samples originating from the excited triplet state disappeared. For example, $[C_{60}]_{0.4}$-ZnPc-COF upon laser flash at 680 nm exhibited a sharp TR-ESR signal. In detail, the TR-ESR signal exhibited an increase up to t = 2.37 ms and then decayed slowly. Therefore, we monitored the TR-ESR spectra at t = 10.0 μs as a function of the magnetic field and obtained a time-sliced magnetic field profile (Figure 3D, red curve). This curve can be reproduced with a single emission-type Lorentzian with a g value of 2.00627 and a narrow spectral width of 0.00132 mT (Figure 3D, black line). The g value of 2.00627 represents the formation of $ZnPc^{\bullet+}$ and $C_{60}^{\bullet-}$ species.[8c] These results indicate that the light irradiation triggers photoinduced electron transfer from ZnPc to fullerene. The narrow spectral width reveals a weak magnetic dipolar interaction between two spins because $ZnPc^{\bullet+}$ and $C_{60}^{\bullet-}$ species are spatially separated. Based on this result, the TR-ESR curve was monitored at 0.3465 T to produce a time profile (Figure 3E, red curve). An exponential function defined by $\Phi = \alpha \exp[-t/\tau_{CS}]$, where α, t, and τ_{CS} are the proportional factor, time, and lifetime, respectively, generates a fitting curve (black curve), which reproduces the experimental curve. The τ_{CS} value was determined to be 2.37 ms.

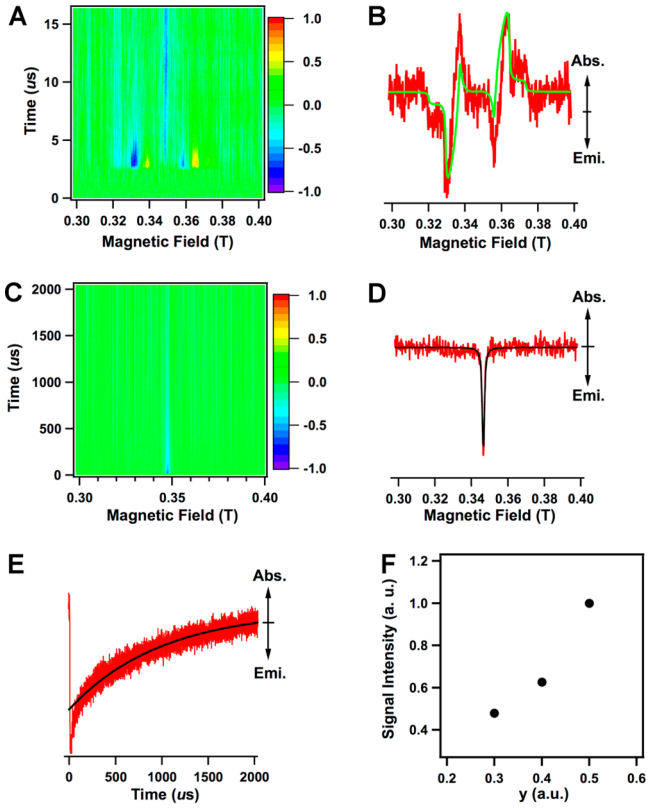

Figure 3. (A) Contour plot of the TR-ESR spectrum of the solid-state ZnPc-COF. (B) Time-sliced TR-ESR spectrum (red) and simulated spectrum (green) of ZnPc-COF. (C) Contour plot of the TR-ESR spectrum of the solid-state $[C_{60}]_{0.4}$-ZnPc-COF. (D) Time-sliced TR-ESR spectrum (red) and simulated spectrum (black) of $[C_{60}]_{0.4}$-ZnPc-COF. (E) Time profile of the TR-ESR signal (red) of $[C_{60}]_{0.4}$-ZnPc-COF. The black line is the curve fitting. (F) Effect of the C_{60} content on the TR-ESR signal intensity.

To elucidate the effect of fullerene content on the charge-separated state, $[C_{60}]_{0.3}$-ZnPc-COF and $[C_{60}]_{0.5}$-ZnPc-COF were subjected to the TR-ESR measurements. $[C_{60}]_{0.3}$-ZnPc-COF exhibited a sharp profile, which gives rise to the g value and spectral width of 2.00666 and 0.00178 mT, respectively (Figure S9). These results indicate that $[C_{60}]_{0.3}$-ZnPc-COF triggers photoinduced charge separation to yield $ZnPc^{\bullet+}$ and $C_{60}^{\bullet-}$ species. The τ_{CS} value was 2.66 ms. As the fullerene content was increased, $[C_{60}]_{0.5}$-ZnPc-COF exhibited the g value and spectral width of 2.00645 and 0.00192 mT, respectively (Figure S10), indicating the generation of $ZnPc^{\bullet+}$ and $C_{60}^{\bullet-}$ species. The τ_{CS} value was 2.49 ms. Therefore, the ordered donor–acceptor structures in the COFs allow photoinduced charge separation in the segregated π-arrays. The similar

dx.doi.org/10.1021/ja502692w | J. Am. Chem. Soc. 2014, 136, 9806–9809

lifetime of charge-separated states observed for $[C_{60}]_y$-ZnPc-COFs suggests that the lifetime is governed by the delocalization of radical cations in the ZnPc columns, whereas the radical anions are localized at C_{60}.

Interestingly, the TR-ESR signal intensity increased as the content of fullerene in $[C_{60}]_y$-ZnPc-COFs was increased (Figure 3F), which indicates that the radical species (charge carriers) are increased in the COFs. This result reflects that the fullerene acceptor is critical for the charge separation; the more the fullerene molecules, the higher the efficiency of the photoinduced electron transfer and charge separation.

In this study, we have developed a method for converting the open structures of COFs into ordered donor−acceptor heterojunctions. In addition to various supramolecular ensembles thus far developed for assembling fullerene-based donor−acceptor systems, our work provides an alternative way to prepare photoelectric systems by exploring channel confinement and lattice ordering. Synthetically, this protocol is general for constructing photoelectric donor−acceptor structures. Functionally, the donor−acceptor heterojunctions are crucial for the photoinduced electron transfer and charge separation, whereas the carrier concentration and charge separation efficiency are dependent on the acceptor content. In this sense, the exploration of COFs with different pore geometry and large pore size is a subject worthy of further investigation. These results suggest the enormous potential of developing COFs for charge separation and photoenergy conversion.

■ ASSOCIATED CONTENT

Supporting Information

Materials and methods, synthetic procedures, Tables S1 and S2, Figures S1−S10. This material is available free of charge via the Internet at http://pubs.acs.org.

■ AUTHOR INFORMATION

Corresponding Author

jiang@ims.ac.jp

Notes

The authors declare no competing financial interest.

■ ACKNOWLEDGMENTS

This work was supported by a Grant-in-Aid for Scientific Research (A) (24245030) from MEXT, Japan.

■ REFERENCES

(1) Feng, X.; Ding, X. S.; Jiang, D. *Chem. Soc. Rev.* **2012**, *41*, 6010.

(2) (a) Côté, A. P.; Benin, A. I.; Ockwig, N. W.; O'Keeffe, M.; Matzger, A. J.; Yaghi, O. M. *Science* **2005**, *310*, 1166. (b) Colson, J. W.; Woll, A. R.; Mukherjee, A.; Levendorf, M. P.; Spitler, E. L.; Shields, V. B.; Spencer, M. G.; Park, J.; Dichtel, W. R. *Science* **2011**, *332*, 228.

(3) (a) Wan, S.; Guo, J.; Kim, J.; Ihee, H.; Jiang, D. *Angew. Chem., Int. Ed.* **2008**, *47*, 8826. (b) Ding, X.; Guo, J.; Feng, X.; Honsho, Y.; Guo, J.; Seki, S.; Maitarad, P.; Saeki, A.; Nagase, S.; Jiang, D. *Angew. Chem., Int. Ed.* **2011**, *50*, 1289. (c) Feng, X.; Chen, L.; Dong, Y.; Jiang, D. *Chem. Commun.* **2011**, *47*, 1979. (d) Ding, X.; Chen, L.; Honsho, Y.; Feng, X.; Saengsawang, O.; Guo, J.; Saeki, A.; Seki, S.; Irle, S.; Nagase, S.; Vudhichai, P.; Jiang, D. *J. Am. Chem. Soc.* **2011**, *133*, 14510. (e) Feng, X.; Liu, L.; Honsho, Y.; Saeki, A.; Seki, S.; Irle, S.; Dong, Y.; Nagai, A.; Jiang, D. *Angew. Chem., Int. Ed.* **2012**, *51*, 2618. (f) Ding, X. S.; Feng, X.; Saeki, A.; Seki, S.; Nagai, A.; Jiang, D. *Chem. Commun.* **2012**, *48*, 8952.

(4) (a) Feng, X.; Chen, L.; Honsho, Y.; Saengsawang, O.; Liu, L.; Wang, L.; Saeki, A.; Irle, S.; Seki, S.; Dong, Y.; Jiang, D. *Adv. Mater.* **2012**, *24*, 3026. (b) Jin, S.; Ding, X. S.; Feng, X.; Supur, M.; Furukawa, K.; Takahashi, S.; Addicoat, M.; El-Khouly, M. E.; Nakamura, T.; Irle, S.; Fukuzumi, S.; Nagai, A.; Jiang, D. *Angew. Chem., Int. Ed.* **2013**, *52*, 2017. (c) Jin, S.; Furukawa, K.; Addicoat, M.; Chen, L.; Takahashi, S.; Irle, S.; Nakamura, T.; Jiang, D. *Chem. Sci.* **2013**, *4*, 4505.

(5) (a) Dogru, M.; Handloser, M.; Auras, F.; Kunz, T.; Medina, D.; Hartschuh, A.; Knochel, P.; Bein, T. *Angew. Chem., Int. Ed.* **2013**, *52*, 2920. (b) Guo, J.; Xu, Y.; Jin, S.; Chen, L.; Kaji, T.; Honsho, Y.; Addicoat, M. A.; Kim, J.; Saeki, A.; Ihee, H.; Seki, S.; Irle, S.; Hiramoto, M.; Gao, J.; Jiang, D. *Nat. Commun.* **2013**, *4*, 2736.

(6) Nagai, A.; Guo, Z. Q.; Feng, X.; Jin, S. B.; Chen, X.; Ding, X. S.; Jiang, D. *Nat. Commun.* **2011**, *2*, 536.

(7) (a) Tilford, R. W.; Mugavero, S. J.; Pellechia, P. J.; Lavigne, J. J. *Adv. Mater.* **2008**, *20*, 2741. (b) Xu, H.; Chen, X.; Gao, J.; Lin, J.; Addicoat, M.; Irle, S.; Jiang, D. *Chem. Commun.* **2014**, *50*, 1292.

(8) (a) Guldi, D. M.; Gouloumis, A.; Vazquez, P.; Torres, T.; Georgakilas, V.; Prato, M. *J. Am. Chem. Soc.* **2005**, *127*, 5811. (b) de la Escosura, A.; Martinez-Diaz, M. V.; Guldi, D. M.; Torres, T. *J. Am. Chem. Soc.* **2006**, *128*, 4112. (c) Niemi, M.; Tkachenko, N. V.; Efimov, A.; Lehtivuori, H.; Ohkubo, K.; Fukuzumi, S.; Lemmetyinen, H. *J. Phys. Chem. A* **2008**, *112*, 6884.